THE JOURNAL OF BIOLOGICAL CHEMISTRY VOL. 283, NO. 27, pp. 18937–18946, July 4, 2008

NMR Analysis of KChIP4a Reveals Structural Basis for Control of Surface Expression of Kv4 Channel Complexes*[S]

Received for publication, February 6, 2008, and in revised form, April 7, 2008 Published, JBC Papers in Press, May 5, 2008, DOI 10.1074/jbc.M800976200

Jochen Schwenk[‡], Gerd Zolles[‡], Nikolaos G. Kandias[§], Isabel Neubauer[‡], Hubert Kalbacher[¶], Manuel Covarrubias[‖], Bernd Fakler[‡], and Detlef Bentrop[‡1]

From the [‡]Institute of Physiology II, University of Freiburg, D-79104 Freiburg, Germany, the [§]Department of Pharmacy, School of Health Sciences, University of Patras, GR-26500 Rion, Patras, Greece, the [¶]Interfacultary Institute for Biochemistry, Medical, and Natural Sciences Research Centre, University of Tübingen, D-72074 Tübingen, Germany, and the [‖]Department of Pathology, Anatomy, and Cell Biology, Jefferson Medical College, Thomas Jefferson University, Philadelphia, Pennsylvania 19107

Potassium channel-interacting proteins (KChIPs) are EF-hand calcium-binding proteins of the recoverin/neuronal calcium sensor 1 family that co-assemble with the pore-forming Kv4 α-subunits and thus control surface trafficking of the voltage-gated potassium channels mediating the neuronal I_A and cardiac I_{to} currents. Different from the other KChIPs, KChIP4a largely reduces surface expression of the Kv4 channel complexes. Using solution NMR we show that the unique N terminus of KChIP4a forms a 6-turn α-helix that is connected to the highly conserved core of the KChIP protein via a solvent-exposed linker. As identified by chemical shift changes, N-terminal α-helix and core domain of KChIP4a interact with each other through the same hydrophobic surface pocket that is involved in intermolecular interaction between the N-terminal helix of Kv4α and KChIP in Kv4-KChIP complexes. Electrophysiological recordings and biochemical interaction assays of complexes formed by wild-type and mutant Kv4α and KChIP4a proteins suggest that competition of these two helical domains for the surface groove is responsible for the reduced trafficking of Kv4-KChIP4a complexes to the plasma membrane. Surface expression of Kv4 complexes may thus be controlled by an autoinhibitory domain in the KChIP subunit.

Potassium channel-interacting proteins (KChIPs)[2] (1) are cytoplasmic EF-hand proteins of the recoverin/neuronal calcium sensor 1 family that interact with the cytoplasmic N and C termini of the pore-forming α-subunits of Kv4 voltage-gated potassium (Kv) channels (Kv4α) (2–5). Together with dipeptidyl-aminopeptidase-like proteins (DPP6 and DPP10) (6, 7), type II transmembrane proteins, KChIPs are integral components of these heteromultimeric Kv channels in brain (KChIPs1–4) and heart (KChIP2) where they act as important regulators of excitability by mediating the somatodendritic A-type current I_A in neurons (8) and the transient outward current I_{to} in cardiac myocytes (9).

KChIPs are Ca^{2+}-binding proteins with a conserved core region of ~180 amino acids and highly variable N termini (~35–100 residues). The core region contains 4 EF-hand motifs comprising 8 helices that are preceded and followed by an additional helix, respectively (5, 10). EF-hands 3 and 4 are canonical Ca^{2+} binding sites in all KChIP isoforms, whereas EF-hand 1 is non-functional because of the lack of key Ca^{2+} coordinating residues. EF-hand 2 in KChIPs2–4 prefers Mg^{2+} over Ca^{2+} because of a Glu to Asp exchange in the last bidentate Ca^{2+} ligand, in KChIP1 EF-hand 2 does not bind divalents as the second and third Ca^{2+}-coordinating residues are substituted by Thr.

Within Kv4 channel complexes, KChIP proteins exert two distinct functional effects observed in heterologous expression systems: first, inactivation gating is markedly altered, and second, surface expression of the Kv4 complexes is largely increased (1). For the latter effect, KChIPs are thought to promote the release of channel complexes from the endoplasmic reticulum (ER) and/or from retention in the Golgi apparatus (11, 12). Accordingly, several studies suggested that the highly conserved N terminus of the Kv4 α-subunits may operate as a retention signal that becomes efficiently masked or disabled by interaction with the KChIPs (2, 5, 13).

Recently, the structural basis of the Kv4-KChIP interaction was elucidated by two essentially identical crystal structures of the KChIP1 core region complexed with the cytoplasmic N terminus of Kv4.3 (14, 15). These structures show a cross-shaped octamer with the T1 domains of Kv4.3 forming a tetramer in the center. Four KChIP1 molecules are arranged laterally such that a single KChIP1 molecule interacts with two neighboring

* This work was supported, in whole or in part, by National Institutes of Health Grant R01 NS032337 from NINDS (to M. C.). This work was also supported by grants from the Deutsche Forschungsgemeinschaft (to B. F.) (SFB 388; GRK 843), and the Access to Research Infrastructures activity in the 6th Framework Program of the EC (Contract RII3-026145, EU-NMR). The costs of publication of this article were defrayed in part by the payment of page charges. This article must therefore be hereby marked "*advertisement*" in accordance with 18 U.S.C. Section 1734 solely to indicate this fact.

[S] The on-line version of this article (available at http://www.jbc.org) contains supplemental Figs. S1–S4.

Chemical shift assignments have been deposited in the Biological Magnetic Resonance Data Bank (BMRB; http://www.bmrb.wisc.edu) with accession codes 15422 (KChIP4a WT) and 15425 (KChIP4a(Δ1–42)).

[1] To whom correspondence should be addressed: Hermann-Herder-Str. 7, D-79104 Freiburg, Germany. Fax: 49-761-2035191; E-mail: detlef.bentrop@physiologie.uni-freiburg.de.

[2] The abbreviations used are: KChIP, potassium channel-interacting protein; Kv, voltage-gated K^+ channel; KIS, K^+ channel inactivation suppressor; T1 domain, cytoplasmic N-terminal tetramerization domain of Kv channels; TROSY, transverse relaxation optimized spectroscopy; NOE, nuclear Overhauser effect; NOESY, NOE spectroscopy; GB1, B1 immunoglobulin binding domain of streptococcal protein G; MOPS, 4-morpholinepropanesulfonic acid; CHAPS, 3-[(3-cholamidopropyl)dimethylammonio]-1-propanesulfonic acid; MES, 4-morpholineethanesulfonic acid; RDCs, residual dipolar couplings; PDB, protein data bank; ER, endoplasmic reticulum; csi, chemical shift index.

T1 domains acting as a clamp to stabilize the tetrameric arrangement of the Kv4.3 T1 domains. As predicted by an earlier study (5) two contact interfaces are involved in the interaction between the KChIP1 core and the cytoplasmic N terminus of Kv4.3. First, the hydrophobic N terminus of Kv4.3 is buried in an elongated pocket formed on the surface of the KChIP1 protein by displacement of its helix 10, *i.e.* helix 10 of KChIP1 changes its position and thus allows for binding of the Kv4.3 N terminus, which adopts a helical conformation in the complex. Second, the same KChIP1 molecule interacts via helix 2 with a loop (residues 70–78) on the surface of an adjacent T1 monomer.

Different from the aforementioned KChIP proteins, KChIP4a, a splice variant of KChIP4, exhibits distinct modulation of Kv4 currents via its unique N terminus (16). These first 34 amino acids act as a modular domain that eliminates fast inactivation of Kv4 complexes (therefore also termed K^+ channel inactivation suppressor (KIS) domain) and abolishes enhanced forward trafficking to the plasma membrane. Accordingly, the surface expression of Kv4 channels was markedly reduced in Kv4-KChIP complexes harboring the KChIP4a protein (13). At present, either action of the KChIP4a N terminus remains mechanistically unclear.

Here we report solution NMR data on KChIP4a indicating that the N-terminal KIS domain forms an extended α-helix, which interacts with and induces conformational rearrangements of the KChIP core domain. As a result, the KIS α-helix gets buried in a hydrophobic surface pocket of the KChIP core similar to what was found for the Kv4.3 N terminus in the KChIP1-Kv4.3 T1 domain complex. Together with electrophysiological and biochemical data, these results provide a simple molecular mechanism for the negative trafficking effect of KChIP4a as well as for the enhanced surface expression of Kv4-KChIP complexes containing the other KChIP proteins.

EXPERIMENTAL PROCEDURES

Protein Expression and Purification—KChIP4a from mouse (Swiss-Prot Q6PHZ8–4) with an N-terminal hexa-His tag was expressed at 30 °C as a soluble protein in *Escherichia coli* BL21(DE3) under control of an isopropyl-1-thio-β-D-galactopyranoside inducible promoter (modified pET16b vector, Novagen). After cell lysis by ultrasonication in 20 mM MOPS, 300 mM NaCl, 4 mM β-mercaptoethanol (pH 7.4), the protein was purified to homogeneity by three chromatographic steps on GE Healthcare columns: metal chelate affinity (Ni-Sepharose), anion-exchange (Mono Q), and size-exclusion (Superdex 75). 2–5 mM *N*-octylglucoside was added to all buffers to maximize the yield of monomeric KChIP4a during purification and to stabilize the protein monomer during NMR measurements. Fractions of KChIP4a monomer were pooled and adjusted to 0.1 mM $CaCl_2$ before sample concentration and buffer exchange for NMR by ultracentrifugation.

The N-terminal deletion mutant KChIP4a(Δ1–42) was expressed with a pET30-based vector as a C-terminal fusion to GB1 protein and purified by the same protocol as wild type. Thrombin cleavage and an additional size-exclusion chromatography yielded the (Δ1–42) deletion mutant with an N-terminal hexa-His tag and five additional residues (GSTMG) as cloning artifact.

Amino acid specific labeling of wild type and the (Δ1–42) deletion mutant with ^{15}N-Lys, -Phe, -Leu, -Ile, and -Val, respectively, was performed according to published protocols (17–19). All uniformly isotope-labeled proteins were expressed on M9 minimal medium of appropriate composition with NH_4Cl and glucose as sole nitrogen and carbon source, respectively.

The GB1-KIS fusion protein was also expressed in *E. coli* BL21(DE3). Cells were lysed by ultrasonication in 20 mM Tris, pH 7.4, 300 mM NaCl. Purification in the presence of 1% CHAPS was achieved via metal chelate affinity and size-exclusion chromatography.

NMR Spectroscopy—Unless otherwise mentioned, all NMR experiments were done with samples containing 10% D_2O (v/v) in 5-mm Shigemi tubes on a Bruker Avance 600 spectrometer equipped with a cryogenically cooled pulsed-field gradient triple-resonance probe (TXI). All samples contained 2,2-dimethyl-2-silapentane-5-sulfonate (DSS) as internal standard for ^{1}H chemical shift referencing.

The NMR measurements of KChIP4a (wild type and Δ1–42) were carried out with samples containing 0.1–0.28 mM ^{2}H/^{13}C/^{15}N-labeled protein in 10 mM MOPS (pH 7.4), 4 mM dithiothreitol, 5 mM *N*-octylglucoside, and 2 mM $MgCl_2$ at 300 K. ^{1}H-^{15}N correlation spectra were usually recorded with the TROSY technique (20). TROSY-based triple-resonance experiments (HNCA, HN(CO)CA, intraHNCA (21), HNCACB, HN(CO)CACB, and HNCO) (22, 23), and a three-dimensional NOESY-^{1}H-^{15}N-TROSY (24) with a mixing time of 120 ms were recorded for the backbone assignment.

^{1}H-^{15}N residual dipolar couplings were determined from a two-dimensional HSQC-IPAP experiment (25) on a ^{15}N-labeled sample of KChIP4a without and with ~10 mg/ml Pf1 phage (Profos AG, Regensburg, Germany). The ^{2}H splitting of the aligned sample was 8.5 Hz. Analysis of the RDCs was done with the software package PALES (26) using an alignment tensor obtained from a singular value decomposition fit (27) and a structural model for the KChIP4a core based on the crystal structure of isolated KChIP1 (5) (PDB entry 1S1E). The latter was produced with SWISS-MODEL (28) using the sequence of the KChIP4a core from mouse (Ala^{51}–Ile^{229}; 79% sequence identity to human KChIP1 in 1S1E).

For wild type, a ^{1}H/^{2}H exchange experiment was performed by dissolving a fully protonated ^{15}N-labeled lyophilized sample in 100% ^2H_2O and recording a series of ^{1}H-^{15}N TROSY spectra. The protection of backbone amide protons from solvent exchange on the ms-s timescale was assessed qualitatively by the absence of a cross peak between the amide proton and water in the ^{15}N-resolved three-dimensional NOESY spectrum (29).

For the backbone assignment of ^{13}C/^{15}N-labeled GB1-KIS in 10 mM MES, 1 mM SDS, 0.05% CHAPS, pH 6.5, the following standard spectra were recorded with a 0.3 mM sample at 305 K: ^{1}H-^{15}N HSQC, HNCA, HN(CO)CA, HNCO, HN(CO)CACB, HNCACB, three-dimensional NOESY-^{1}H-^{15}N-HSQC with a mixing time of 100 ms. Additionally, a 100-ms NOESY-^{1}H-^{15}N-TROSY and TROSY-HNCA, -HN(CO)CA, -CBCANH were acquired at 291 K, pH 7.4, in 10 mM MOPS buffer containing the same detergents. All NMR data were processed with the

Bruker XWINNMR or TOPSPIN software and analyzed with the programs XEASY (30) and CARA (available free of charge from www.nmr.ch) (31).

Docking—The standard docking protocol of HADDOCK 1.3 (32) including explicit water refinement was used to calculate a structural model of KChIP4a without the flexible linker between the KIS helix and the KChIP core. Starting structures were the KChIP1 structure in the KChIP1-Kv4.3T1 complex (14) (PDB entry 2I2R, chain E) and an α-helix corresponding to Glu^{4}–Gln^{25} of KChIP4a. The interacting interface of KChIP was defined according to the full set of NMR chemical shift perturbation data. Ambiguous interaction restraints between this surface and the entire KIS helix were used. As expected, due to the absence of experimental restraints for residues of the KIS helix, the orientation of the latter in the hydrophobic groove of the KChIP core is ambiguous. All figures showing structures were prepared with MOLMOL (33).

Affinity Purification and Western Blotting—Three days after injection *Xenopus laevis* oocytes were homogenized with potters in 0.5 ml of 10 mM HEPES pH 7.4, 83 mM NaCl, 1 mM $MgCl_2$,1 mM EGTA, 1 mM iodacetamide (with protease inhibitors), and centrifuged for 10 min at 100 × *g* and 300 × *g* to remove yolk and material from nuclei. Crude membrane preparations were obtained from the homogenates by ultracentrifugation (20 min at 125,000 × *g*). Membranes were solubilized using ComplexioLyte48 (1 ml/mg of membrane protein) (34) and subjected to analytical affinity purification (AP). Total amount of protein used for AP was estimated to equal that of the Kv4.3 protein. Briefly, the solubilized material (0.1–0.4 mg) was incubated for 2 h at 4 °C with 5 μg of immobilized affinity-purified rabbit anti-Kv4.3 (Alomone, APC-017). After washing, bound proteins were eluted with Laemmli buffer (dithiothreitol added after elution) followed by 7.5%/15%-SDS-PAGE and electroblotting on polyvinylidene difluoride membrane. The blot was subjected to Western analysis with mouse anti-Kv4.3 (kind gift of Dr. J. Trimmer) and mouse anti-pan-KChIP (NeuroMab); antibody-stained bands were visualized by anti-mouse IgG-HRP (Santa Cruz) and ECL+.

Electrophysiology and Data Evaluation—Preparation and injection of cRNA into *Xenopus* oocytes and site-directed mutagenesis were done as described (35). All cDNAs and mutants were verified by sequencing; GenBank™ accession numbers of the Kv.4.3 and KChIP4a cDNAs used are AF334791 and AF453243.1, respectively. N-terminal mutations were as follows: KChIP4a-delN indicates deletion of amino acids 2–42 in KChIP4a, Kv4.3-delN denotes deletion of residues 2–22 in Kv4.3, Kv4.3-delN+KIS is a replacement of amino acids 1–22 in Kv4.3 by the first 44 residues of KChIP4a.

Electrophysiological recordings from giant inside-out patches excised from oocytes were performed at room temperature (22–24 °C) as described previously (35). Briefly, currents were recorded with an EPC9 amplifier, low-pass filtered at 1–3 kHz, and sampled at 5–10 kHz; capacitive transients were compensated with the automated circuit of the EPC9. Pipettes made from thick-walled borosilicate glass had resistances of ~0.3 MOhm when filled with (in mM) 115 NaCl, 5 KCl, 5 HEPES, and 1.3 $CaCl_2$, pH adjusted to 7.2. Intracellular solution (K_{int}) applied via a gravity-driven multi-barrel pipette was composed as follows (mM): 120 KCl, 5 HEPES, 1 EGTA (pH 7.2). The inactivation time course of currents mediated by Kv4.3 and Kv.4.3-KChIP4a complexes was characterized by the time constant ($\tau_{inactivation}$) derived from a monoexponential fit to the decay phase of the current. Curve fitting and further data analysis were done with Igor Pro 4.05A on a Macintosh G4. Data are given as mean ± S.D. throughout the report.

RESULTS

Structural Properties and Metal Binding of KChIP4a—KChIP4a was expressed in *E. coli* as a soluble and uniformly isotope ($^{2}H/^{13}C/^{15}N$)-labeled protein, purified to homogeneity and used for structural analyses by NMR in solution (for details see "Experimental Procedures"). Initial two-dimensional ^{1}H-^{15}N correlation experiments with transverse relaxation-optimized spectroscopy (TROSY) (20) showed that the KChIP4a protein exhibited stable tertiary folding only upon addition of Ca^{2+} (0.1 mM) and Mg^{2+} (2 mM), while apoKChIP4a adopted an unstructured state similar to what was seen in recent studies on yeast frequenin and KChIP3 (36, 37). Fig. 1*A* illustrates such a two-dimensional ^{1}H-^{15}N TROSY spectrum of the divalent-loaded KChIP4a, with the peaks representing main-chain and side-chain amide groups. The chemical shift dispersion was about 4 ppm, with some overlap of peaks in the middle of the spectrum indicating exchange broadening for a number of residues as a result of conformational heterogeneity of some parts of the protein. Out of the 224 non-proline amino acids of KChIP4a 204 were detected in the spectrum in Fig. 1*A*. A total of 161 residues (72%) were assigned sequence-specifically using sequential connectivities from TROSY versions of standard triple-resonance spectra, a three-dimensional ^{15}N-resolved NOESY-TROSY experiment and ^{1}H-^{15}N TROSY spectra of KChIP4a proteins with amino acid-specific ^{15}N labeling (for Val, Leu, Ile, Lys, and Phe, respectively; Fig. 1*A* and Fig. 2*A*).

Based on this assignment, the solution structure of KChIP4a and the binding of divalent cations to the EF-hand motifs were analyzed. As shown in Fig. 1, *B–D*, the conserved glycine residues at the sixth position of the EF-hand loops display distinct chemical shifts of their amide protons between 10 and 11 ppm depending on the divalent cation bound. Thus, EF-hand 2 (represented by Gly^{117}) binds Mg^{2+}, whereas EF-hands 3 (Gly^{153}) and 4 (Gly^{201}) are high affinity Ca^{2+} binding sites, implying that under physiological conditions (1–2 mM Mg^{2+},$\ll 10^{-4}$ M Ca^{2+}) KChIP4a may exist either in the 3 Mg^{2+} or in the 2 Ca^{2+}/1 Mg^{2+} state.

Analysis of the Cα chemical shifts (38) together with NOE cross peaks between adjacent backbone amide protons ($^{1}H^{N}_{i}$-$^{1}H^{N}_{i+1}$) identified a series of α-helices and short β-strands in the core region of KChIP4a (residues 51–229; Fig. 2*A*) whose extension and localization closely resembled the respective secondary structure elements in the crystal structure of KChIP1 (5, 10). The only missing elements were the β-strand and the second helix of EF-hand 1 (Val^{82}–Ser^{92}) that could not be assigned through NMR spectra, and a short 3_{10} helix (Pro^{177}–Leu^{179}) in the loop between EF-hands 3 and 4 (Fig. 2*A*).

Extensive formation of secondary structure that is stabilized by hydrogen bonds was further corroborated by the observation of slow exchange of backbone amide protons with the sol-

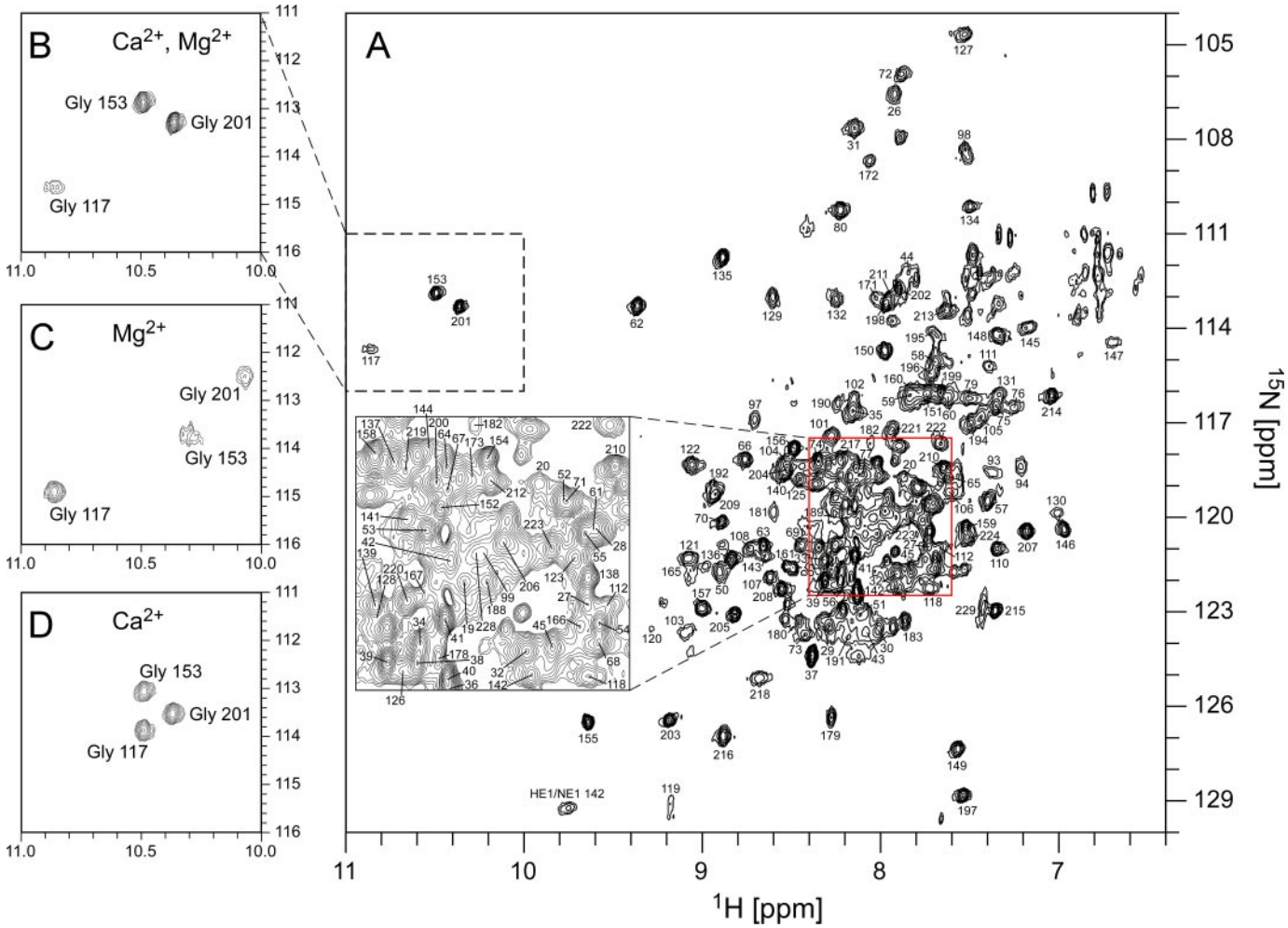

FIGURE 1. **Two-dimensional ^{1}H-^{15}N TROSY correlation spectrum and metal loading of KChIP4a.** *A*, full spectrum of the Ca^{2+}- and Mg^{2+}-loaded KChIP4a protein with assignment of cross peaks to backbone amide groups. Inset displays the indicated part of the spectrum at enlarged scale. HE1/NE1 142 refers to the side chain amide group of Trp^{142}. *B–D*, details of ^{1}H-^{15}N TROSY spectra of KChIP4a showing the cross peaks of the glycine residues in EF-hands 2–4 observed with different divalent cations bound. *B* is the 2 Ca^{2+}, 1 Mg^{2+} state as in *A*; *C* is the 3 Mg^{2+} state (obtained in the absence of Ca^{2+}, but with 2.1 mM Mg^{2+}); *D* represents the 3 Ca^{2+} state (in the absence of Mg^{2+}, but with 2.0 mM Ca^{2+}). The spectrum in *A* and *B* was recorded on a ^{2}H/^{13}C/^{15}N labeled sample, the spectra in *C* and *D* with ^{15}N-labeled samples.

vent. Thus, on the millisecond-to-second timescale the vast majority of assigned KChIP4a residues are protected from solvent exchange as seen from the absence of cross peaks between the amide proton and water in the ^{15}N-resolved three-dimensional NOESY spectrum (*unshaded residues* in Fig. 2*A*) (29). The only contiguous stretch of readily solvent-accessible residues was found between Glu^{29} and Met^{42}, a negatively charged sequence without secondary structure connecting the hydrophobic part of the KIS domain to the core region of KChIP4a. Importantly, the residues in this stretch give rise to some of the most intense peaks in the ^{1}H-^{15}N TROSY (Fig. 1*A*), and their Hα resonances were easily assigned from strong cross peaks in a three-dimensional HNHA spectrum on a sample of ^{15}N-labeled KChIP4a implying that their rotational correlation time is significantly shorter than for the rest of the protein. A series of amino acids, particularly in the C-terminal-half of KChIP4a, exhibited ^{1}H/^{2}H exchange times on the hours-to-days timescale (*diamonds* in Fig. 2*A*) indicating stable and compact folding of the part of the protein harboring EF-hands 3 and 4 (Fig. 2*A*).

In addition to secondary structure elements, NMR analyses provided information on the tertiary structure of KChIP4a. First, two long-range NOEs were observed in the ^{15}N-resolved three-dimensional NOESY spectrum between the amide protons of Val^{82} (EF-hand 1) and Val^{119} (EF-hand 2), and between Ile^{155} (EF-hand 3) and Val^{203} (EF-hand 4), respectively. In fact, these are the only long-range NOEs between amide protons that are predicted by the crystal structure of isolated KChIP1 (5) and they define the short two-stranded β-sheets typically observed in EF-hand proteins; other NOEs were not detectable due to the required deuteration of the samples. Second, ^{1}H-^{15}N residual dipolar couplings (RDCs) (39–41) were measured to identify the fold of the KChIP4a core region (Ala^{51}–Ile^{229}). For this analysis only RDCs of well-resolved residues with sufficiently high signal-to-noise ratio in the HSQC-IPAP spectra were used. Moreover, residues in putatively unstructured or flexible regions as judged by the random coil index (42, 43) were excluded. Finally, the RDC values of 73 residues (53% of 138 assigned residues in the KChIP4a core region) that represent the secondary structure elements between Leu^{52} and Leu^{224}

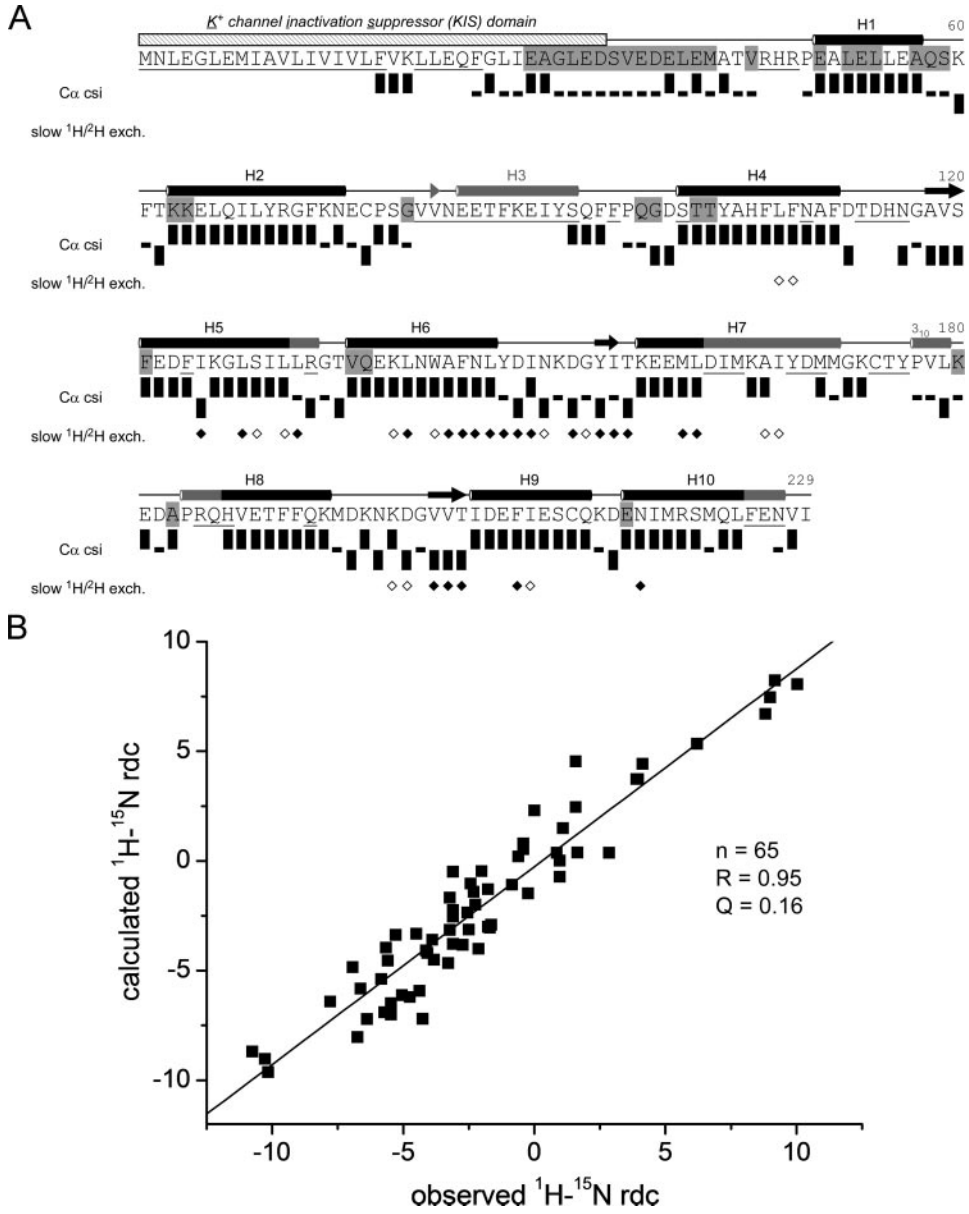

FIGURE 2. **NMR data on secondary structure and tertiary folding of KChIP4a.** *A*, sequence, secondary structure, and schematic representation of NMR data of KChIP4a. The KIS domain is indicated by a *hatched bar*. Secondary structure elements determined by NMR and for the crystal structure of KChIP1 (5) are indicated by *black* and *gray symbols*, respectively. *Cylinders* represent helices (H1-H10), *arrows* are short β-strands in the metal-binding loops of the EF-hands. Residues whose backbone amide group was not assigned are *underlined*; residues not protected from solvent exchange on the ms-s timescale are highlighted in *gray*. Cα chemical shift index (*csi*) (38) (values were corrected for ^{2}H isotope effects (48, 49)) identifies secondary structures of KChIP4a: *Upright bars* reflect a csi value of +1 (typical for α-helices), *bars* with downward orientation represent a csi value of −1 (typical for β-strands), *small black rectangles* represent a csi value of 0 (chemical shifts similar to random coil values). *Diamonds* summarize a ^{1}H/^{2}H exchange experiment: *open* and *filled symbols* correspond to residues with amide protons still present after 90 min and 28 h of exchange time in 100% ^2H_2O, respectively. *B*, analysis of ^{1}H-^{15}N residual dipolar couplings (RDCs) of KChIP4a. Correlation between observed ^{1}H-^{15}N RDCs and couplings predicted for a structural model of the KChIP4a core based on the 2.3 Å x-ray structure of isolated KChIP1 (5) (PDB entry 1S1E). The analysis was done with the PALES program (26). Alignment tensor relative to the model: D_a^{NH} = 6.4 Hz and rhombicity r = 0.35.

were compared with those back-calculated from the KChIP1 crystal structure. Surprisingly, fit of the data yielded a poor quality factor Q = 0.36 (regression coefficient R = 0.82) with residues in helix H10 showing the biggest differences between observed and back-calculated RDCs. However, when the RDCs of Glu^{216}, Asn^{217}, Ile^{218}, Arg^{220}, Ser^{221}, Met^{222}, Gln^{223}, and Leu^{224} in H10 were excluded from the analysis, the quality of the fit was markedly improved (Q = 0.16, Fig. 2*B*) strongly suggesting that H1-H9 of KChIP4a have the same spatial arrangement as in KChIP1, while the orientation of H10 is different.

Together, these results indicated that the solution structure of KChIP4a is very similar in secondary and tertiary folding to the crystal structure of the isolated KChIP1, with differences in the orientation of helix H10 and a flexible solvent-exposed linker to the KIS domain at the N terminus.

Structural Properties of KChIP4a-(Δ1–42) and Structural Rearrangements Induced by the KIS Domain—As the NMR spectra of KChIP4a did not provide direct structural information on its N-terminal KIS domain, a divide-and-conquer approach together with chemical shift perturbation analysis was used to determine its position on the conserved KChIP4a core. For this purpose the N-terminal 42 amino acids of KChIP4a were deleted, and the resulting mutant protein (KChIP4a(Δ1–42)) representing the conserved KChIP core was expressed in *E. coli* and analyzed under the same conditions as the wild-type protein. An identical approach was used recently for identification of the potential contact site between the tetramerization domain of *Aplysia* Kv1.1 channel and its flexible N-terminal tail (44).

The two-dimensional ^{1}H-^{15}N TROSY spectrum of the Ca^{2+}- and Mg^{2+}-loaded KChIP4a(Δ1–42) (Fig. 3*A*) showed that chemical shift dispersion, conformational exchange phenomena and the cross peaks of Gly117, 153, and 201 in EF-hands 2–4 were very similar to wild type. Moreover, the Cα chemical shifts of the 135 assigned residues of KChIP4a(Δ1–42) (= 74% of non-proline residues) identified the same secondary structure elements as in wild type with complementation of some missing stretches including the β-strand and helix H3 of EF-hand 1 and part of helix H7 of EF-hand 3 (Fig. 3*B*). In addition, both long-range NOEs between backbone amide protons in the two short β-sheets (see above) were unambiguously detected in the three-dimensional NOESY spectrum of KChIP4a(Δ1–42), and both wild-type and mutant

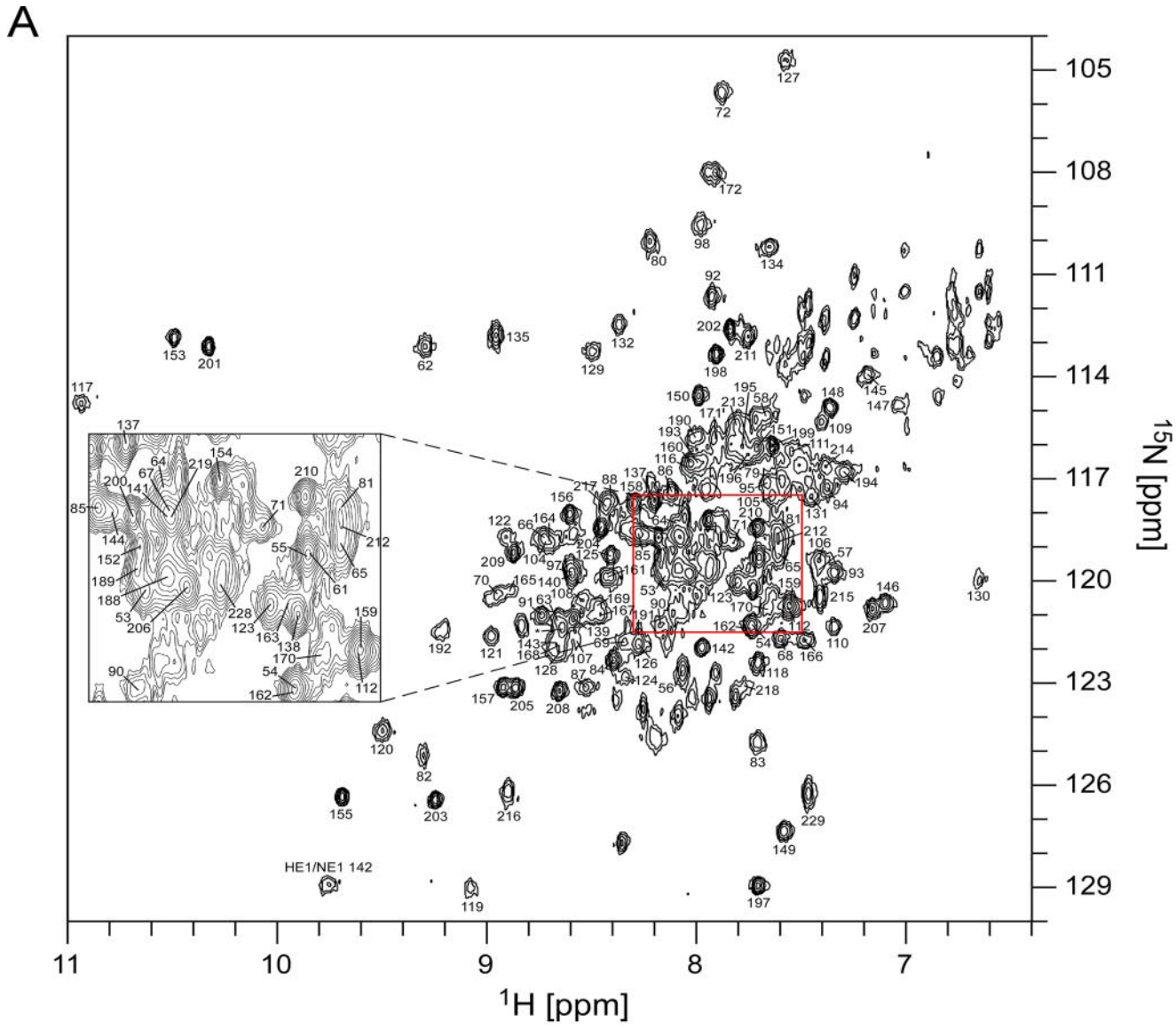
A
105
108
111
114
117
120
123
126
129
15N [ppm]
11
10
9
8
7
1H [ppm]
HE1/NE1 142
B
43
H1
60
ATVRHRPEALELLEAQSK
Cα csi
H2
H3
H4
120
FTKKELQILYRGFKNECPSGVVNEETFKEIYSQFFPQGDSTTYAHFLFNAFDTDHNGAVS
Cα csi
H5
H6
H7
3₁₀
180
FEDFIKGLSILLRGTVQEKLNWAFNLYDINKDGYITKEEMLDIMKAIYDMMGKCTYPVLK
Cα csi
H8
H9
H10
229
EDAPRQHVETFFQKMDKNKDGVVTIDEFIESCQKDENIMRSMQLFENVI
Cα csi

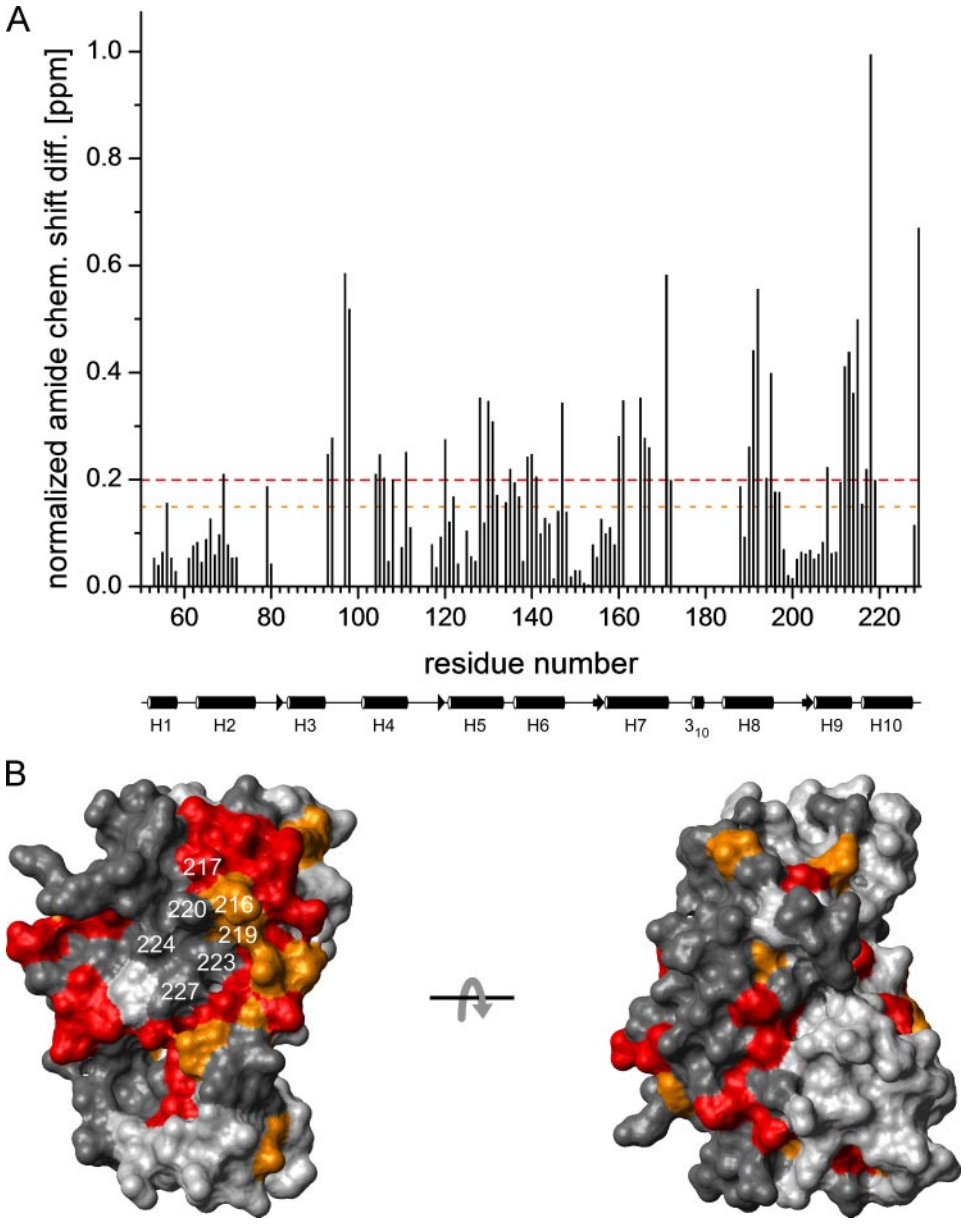

FIGURE 4. **Intramolecular binding site of the KIS domain on the surface of the KChIP4a core identified by chemical shift mapping.** *A*, plot of the normalized backbone amide chemical shift differences (= $[\Delta\delta(^1H)^2 + (0.2\ \Delta\delta(^{15}N))^2]^{1/2}$) (44) between KChIP4a and KChIP4a(Δ1–42) as a function of residue number. The average value is 0.18 ppm. *Dashed lines* in *red* and *orange* indicate differences of 0.2 and 0.15 ppm, respectively. A schematic representation of the secondary structure of the KChIP core with helices H1-H10 is shown *below* the abscissa. *B*, surface representation of a structural model (see Fig. 2*B*) of the KChIP4a core. Residues with chemical shift changes >0.2 ppm are shown in *red*, those with chemical shift changes between 0.15 and 0.2 ppm are in *orange*. Residues for which no chemical shift difference is available are in *dark gray*. H10 residues are identified by their sequence numbers. The two views are related by a 180° rotation around the *x*-axis. Note the large contiguous surface patch on one side of the molecule that most likely delineates the interaction site between the core region of KChIP4a and the KIS domain.

KChIP4a displayed similar protection from solvent exchange on the millisecond-to-second timescale. Together, the secondary structure and the overall tertiary folding of KChIP4a appeared unaffected by deletion of its N-terminal 42 amino acids.

Closer comparison of the two proteins by chemical shift perturbation analysis, however, revealed that a number of residues in the KChIP core structure are markedly affected by the KIS domain. Thus, out of 113 corresponding amide groups assigned in both wild-type and deletion mutant of KChIP4a, a total of 37 showed normalized chemical shift differences of more than 0.2 ppm, and for additional 15 residues values between 0.15 and 0.2 ppm were obtained (Fig. 4*A*). As illustrated in Fig. 4*A*, the two largest chemical shift differences occurred at the C terminus within a cluster formed by numerous residues in the sequential range 188–229 (H8-H10). Interestingly, most of the residues with shift differences > 0.15 ppm were hydrophobic. When all residues with such chemical shift differences between KChIP4a and KChIP4a(Δ1–42) were mapped onto the surface of a structural model of the KChIP4a core (residues 51–229) based on the isolated KChIP1 crystal structure, they formed a prominent contiguous patch on one side of the protein (Fig. 4*B*). Note that part of this patch was covered by H10 (residues 217–227) in this representation (cf. Fig. 6*A*). The reverse side of the molecule was much less affected (Fig. 4*B*).

These data indicated that the hydrophobic KIS domain induces structural changes in the core domain of KChIP4a predominantly in H8 through H10 that may serve as the contact site between the KIS domain and core region.

Solution Structure of the KIS Domain and Its Interaction with the Core Region of KChIP4a—Next, we analyzed the solution structure of the KIS domain, amino acids 1–34 of KChIP4a. Because a chemically synthesized KIS peptide was not suitable for NMR studies due to its poor solubility, it was expressed as a GB1 fusion protein (45) in *E. coli* and purified to homogeneity. Standard triple-resonance experiments allowed for complete backbone assignment of the fusion protein and confirmed the structural integ-

FIGURE 3. **Structural analysis of the KIS-deletion protein KChIP4a(Δ1–42).** *A*, ^1H-^{15}N TROSY spectrum of the Ca^{2+} and Mg^{2+}-loaded KChIP4a(Δ1–42) as in Fig. 1*A*. The cross peak at 8.64/121.45 ppm marked with an *asterisk* corresponds to Val^{136}. *B*, sequence, secondary structure, and schematic representation of NMR data of KChIP4a(Δ1–42) as in Fig. 2*A*.

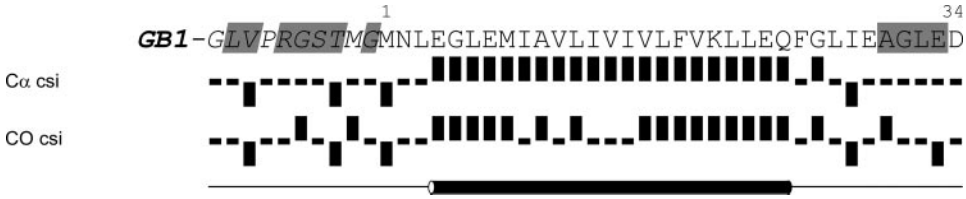

FIGURE 5. **The KIS domain of KChIP4a forms a long α-helix.** Secondary structure of the KIS domain in the GB1-KIS fusion construct. Sequence and chemical shift index for Cα and carbonyl carbons (38) as indicated. The linker between GB1 and the KIS domain is in *italic*. Residues highlighted in *gray* are not protected from amide proton exchange with water. The chemical shift index shows a α-helix extending from Glu[4] through Gln[24].

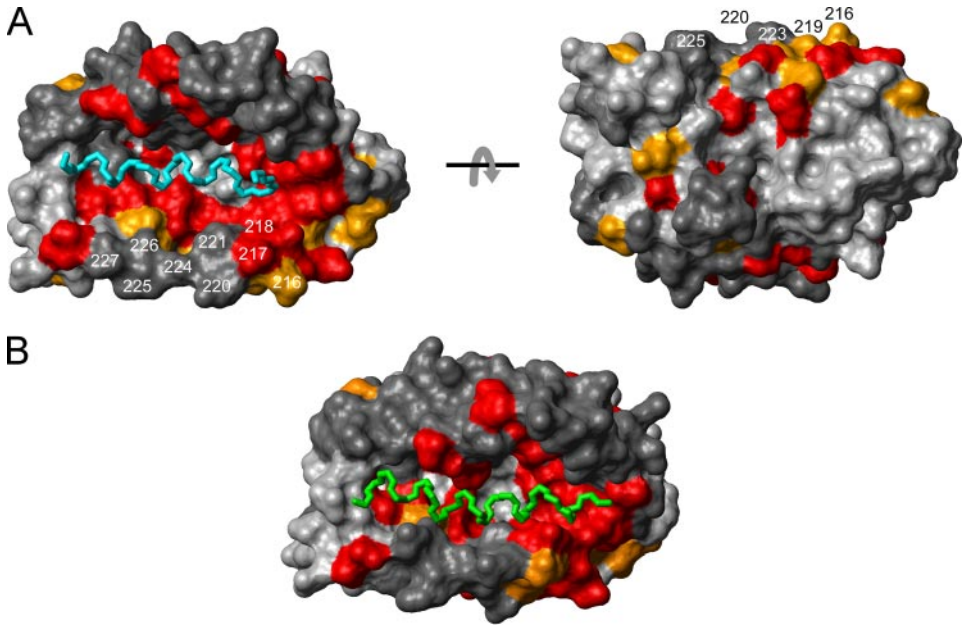

FIGURE 6. **The α-helices of the KIS domain and the Kv4.3 N terminus can bind to the same surface pocket on the KChIP core structure.** *A*, mapping of the NMR chemical shift perturbation data (Fig. 4*A*) onto a surface representation of KChIP1 in the KChIP1-Kv4.3 N terminus x-ray structure (14) (PDB entry 2I2R). Color coding and residue numbers in the KChIP4a numbering system are as in Fig. 4*B*. The two views are related by a 180° rotation around the *x*-axis. The main chain of the α-helical segment of the Kv4.3 N terminus buried in the hydrophobic groove of KChIP1 is shown in *cyan* (Ala[3]–Met[20]). *B*, chemical shift-driven docking of the KIS domain α-helix (*green*) to the same KChIP1 structure as in *A*. The docking was performed with HADDOCK 1.3 (32).

rity of the GB1 part (data not shown). Secondary chemical shifts of Cα and carbonyl carbons (CO) (38) and protection from solvent exchange showed that the KIS domain consists of a long α-helix extending from Glu[4] through Gln[24] (Fig. 5) and the flexible solvent-exposed linker described above (Fig. 2). The 10-residue linker between GB1 and the KIS sequence did not adopt any secondary structure and displayed pronounced solvent accessibility.

These results together with the chemical shift perturbation analysis (Fig. 4) indicated that the hydrophobic N terminus of KChIP4a is made up of an extended α-helix that contacts the conserved core domain on a large surface patch. A similar, but intermolecular interaction was recently observed in the crystal structure of the KChIP1-Kv4.3 N-terminal domain complex (14, 15). An N-terminal α-helix of Kv4.3 was found buried in a hydrophobic pocket that formed on the surface of the KChIP1 core as a result of displacement of helix H10. Fig. 6*A* illustrates this surface pocket of KChIP1 together with a mapping of the chemical shift perturbations induced by the hydrophobic KIS domain on the KChIP4a core (Fig. 4*A*). Strikingly, the lining of the surface pocket largely coincides with the residues of the KChIP4a core that experience large chemical shift changes upon interaction with the KIS domain (Fig. 4*A*) implying that the helical segments of both the KIS domain and the Kv4.3 N terminus bind to the same hydrophobic surface pocket on the KChIP core. To support this notion HADDOCK (32) was used to simulate the intramolecular interaction between the KChIP4a core and the KIS domain. A chemical shift-driven docking (see "Experimental Procedures") showed that the hydrophobic groove opened up by displacement of H10 is large enough to accommodate the long KIS domain α-helix (Fig. 6*B*). Because of the length of the linker peptide (Glu[29]–Pro[49]) and the absence of interaction restraints for the residues of the KIS helix the orientation of the latter could not be defined.

Significance of the N Termini of Kv4.3 and KChIP4a for Complex Formation and Surface Trafficking—The result of a potential common binding site for the KIS domain and the Kv4.3 N terminus on the KChIP core was further probed and tested for its functional significance in biochemical and electrophysiological analyses on Kv4 channel complexes synthetically reconstituted in *Xenopus* oocytes. Kv4.3-KChIP complexes were affinity-purified from crude membrane preparations and subsequently separated on SDS-PAGE gels. As illustrated in Fig. 7*A*, complex formation with KChIP4a was observed for wild-type Kv4.3, but also for a mutant of Kv4.3 where the N terminus was replaced by the KIS domain (Kv4.3-delN+KIS). In contrast, no stable assembly was obtained after deletion of the N terminus of Kv4.3 (Kv4.3-delN; Fig. 7*A*). These results indicated that the N terminus of Kv4.3 and the KIS domain promoted complex assembly equivalently, in line with both helical segments binding to the same surface pocket on the KChIP4a core.

Next, the functional significance of the KIS domain was tested by selective monitoring of amount and properties of Kv4.3-KChIP4a complexes in the plasma membrane via electrophysiological measurements. Recordings in excised patch configuration and whole-oocyte voltage clamp showed that association of Kv4.3 channels with KChIP4a reduced the K^+ currents by about 2-fold, while complex formation with the KIS-deleted KChIP4a-delN (= KChIP4a(Δ2–42)) mutant (Fig. 7*A*) lead to a 4–5-fold increase in current amplitude (Fig. 7*C*). An identical increase in current was obtained with Kv4.3 chan-

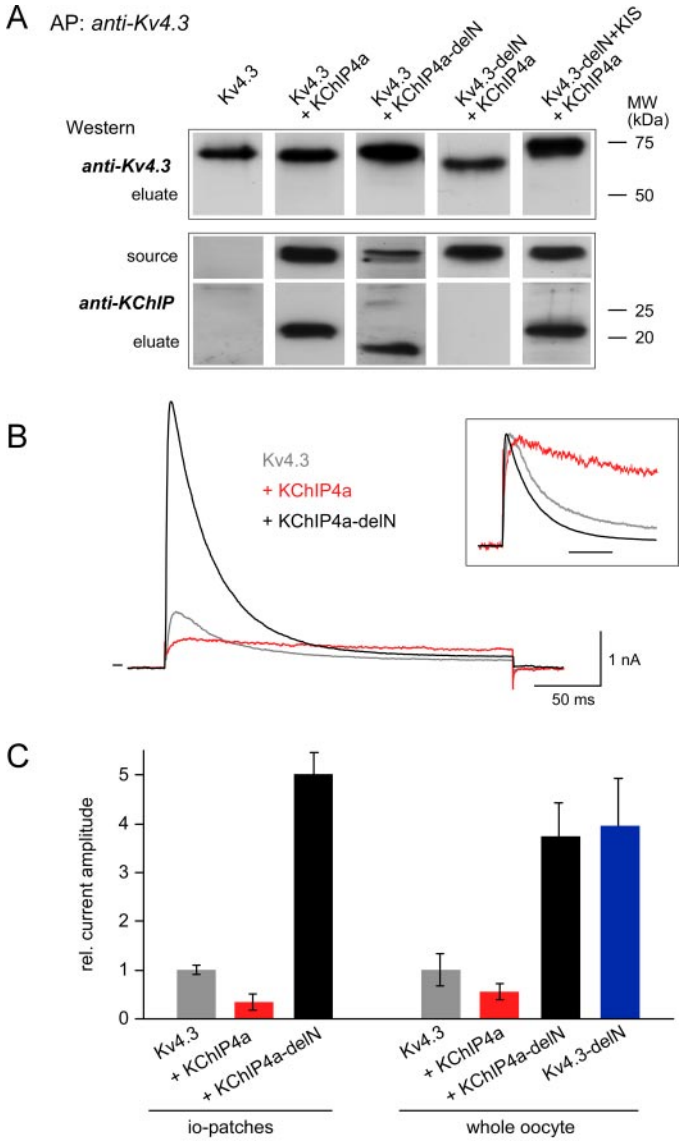

FIGURE 7. **Significance of the helical KIS domain for assembly and surface expression of Kv4.3-KChIP4a complexes.** *A*, formation of Kv4.3-KChIP4a complexes required the core domain of KChIP and a helical segment in the N terminus of Kv4.3. Eluates from affinity purifications (*AP*) with an anti-Kv4.3 antibody from crude membrane preparations of oocytes co-expressing the indicated proteins were separated by SDS-PAGE and Western-probed with anti-Kv4.3 or an antibody targeting the core domain of KChIPs (anti-KChIP). Total amount of protein used for the AP was estimated to equal that of the Kv4.3 protein. *Source* represents the AP-input Western-probed with anti-KChIP. Molecular weight scales for eluates are as indicated. *B*, current responses to 250-ms voltage steps from −80 to 50 mV recorded in giant inside-out patches excised from *Xenopus* oocytes expressing Kv4.3 or co-expressing Kv4.3 and either KChIP4a or the KIS-deleted mutant KChIP4a-delN. *Inset*, current traces normalized to the peak outward current; timescale is 50 ms. *C*, *bar diagram* representing the peak current amplitude recorded from whole oocytes (*right panel*) or in inside-out patches (*left panel*) excised from oocytes expressing the indicated channels or channel complexes. Values are mean ± S.D. of 6–8 oocytes or 8 inside-out patches; current amplitudes were normalized to the mean value determined for homomeric Kv4.3 channels. Note the marked increase in current amplitude observed upon deletion of the KIS domain.

nels after deletion of their N terminus (Fig. 7*C*) in agreement with its assumed operation as an ER retention motif (2, 5).

In addition to the marked changes in surface expression, assembly with the KChIP4a proteins impacted on the gating properties of the channels. Thus, wild-type KChIP4a largely slowed inactivation of Kv4.3 channels (16), while co-assembly of Kv4.3 with the KIS-deleted mutant slightly accelerated channel inactivation (Fig. 7*B*). The respective time constants ($\tau_{inactivation}$, mean ± S.D. of *n* inside-out patches) obtained from monoexponential fits to current responses recorded at 10 mV were 51.9 ± 5.6 ($n = 5$) for Kv4.3 and 37.2 ± 3.8 ($n = 5$) for Kv4.3-KChIP4a-delN.

Together, these results indicated that the prominent increase in surface expression of Kv4.3 channels is mediated by co-assembly with the KChIP core most likely via masking of the ER- or Golgi-retention motif inherent in the Kv4.3 N terminus. This masking is effectively counteracted by addition of the KIS domain to the KChIP core.

DISCUSSION

The central finding of this work is that the KIS domain of KChIP4a forms an extended α-helix that folds back onto the core region of the protein, where it binds to the same hydrophobic surface pocket recently shown to harbor the N-terminal α-helix of Kv4.3 in a KChIP1-Kv4.3 T1 complex (14, 15). In either case, the binding pocket is pushed open by the respective α-helix through displacement of the H10 helix in the KChIP core (14, 15) (Fig. 4). Functionally, the KIS-to-core binding abolishes the increased surface expression mediated by the core domain of all KChIPs (1, 10, 16, 46) (Fig. 7) most likely by competition of the helical segments in both KIS domain and Kv4.3 N terminus for the hydrophobic surface pocket on the KChIP core (Fig. 6).

Such a competition is strongly indicated by NMR titration experiments in which chemically synthesized unlabeled Kv4.3(1–40) peptide (solution structure in supplemental Fig. S1) was added to ^{15}N-labeled KChIP4a. Numerous small chemical shift changes and general line broadening of the peaks in the ^{1}H-^{15}N TROSY spectra of the protein (supplemental Fig. S2) precluded definition of the interaction interface. The only KChIP4a residues clearly not affected by addition of the peptide were Asp^{34}–Val^{45} in the flexible solvent-exposed linker between the KIS domain and the KChIP core. These results suggest a highly complex interaction on different NMR time scales between the isolated Kv4.3 N-terminal peptide and KChIP4a. For example, multiple equilibria may be anticipated if three, more, or less hydrophobic helical segments (namely helix H10, KIS domain, and the N-terminal helix of Kv4.3) compete for hydrophobic surface area on a KChIP molecule. A similar situation was observed in an analogous titration experiment with KChIP4a(Δ1–42) (supplemental Fig. S3).

In vivo this competition should become effective during assembly of channel complexes in intracellular compartments (ER and/or Golgi apparatus) whenever a (newly synthesized) KIS-to-core bound KChIP4a protein hits a Kv4.3 channel subunit. Structurally, this may have two distinct consequences. First, the hydrophobic KIS helix remains bound in the deep surface pocket of the KChIP core and allows for binding of the α-helical segment of the Kv4.3 protein on top of it, or the KIS helix is pushed out of the surface groove and is replaced by the N-terminal helix of Kv4.3. In the first case, the Kv4.3 N terminus will be exposed on the surface ready for interaction with the retention apparatus in ER and/or Golgi finally resulting in

largely reduced surface expression of channel complexes. In the second case, the negative trafficking effect will result from the helix-helix replacement leading to a mixed competitive/allosteric inhibition that generates less channel complexes for anterograde transport to the plasma membrane. Independent of how exactly the helix-helix competition works out structurally, it provides a straightforward explanation for the dominance of the negative trafficking effect of KChIP4a observed in titrated co-expression of KChIP isoforms 2 and 4a with Kv4.3 (13). Thus, any KChIP4a subunit integrating into a channel complex will expose a Kv4.3 N terminus ready to impair the surface trafficking of the channel.

Different from the effect on surface expression, the results presented here do not offer insights into the different effects of KChIP4a on channel activation (supplemental Fig. S4) and inactivation (Fig. 7), that occur most likely through allosteric mechanism(s) (12, 47). Comprehensive understanding of these effects of KChIP proteins on channel gating may require crystal data of the entire Kv4-KChIP heterooctamer.

Acknowledgments—We thank Drs. V. Dötsch (Frankfurt) for his advice on protein expression and site-specific labeling, J. Trimmer (Davis, CA) for antibodies, G. Spyroulias (Patras) for help with HADDOCK, and U. Schulte and N. Klöcker for discussion and reading of the manuscript.

REFERENCES

1. An, W. F., Bowlby, M. R., Betty, M., Cao, J., Ling, H. P., Mendoza, G., Hinson, J. W., Mattsson, K. I., Strassle, B. W., Trimmer, J. S., and Rhodes, K. J. (2000) *Nature* **403,** 553–556
2. Bahring, R., Dannenberg, J., Peters, H. C., Leicher, T., Pongs, O., and Isbrandt, D. (2001) *J. Biol. Chem.* **276,** 23888–23894
3. Callsen, B., Isbrandt, D., Sauter, K., Hartmann, L. S., Pongs, O., and Bahring, R. (2005) *J. Physiol.* **568,** 397–412
4. Han, W., Nattel, S., Noguchi, T., and Shrier, A. (2006) *J. Biol. Chem.* **281,** 27134–27144
5. Scannevin, R. H., Wang, K., Jow, F., Megules, J., Kopsco, D. C., Edris, W., Carroll, K. C., Lu, Q., Xu, W., Xu, Z., Katz, A. H., Olland, S., Lin, L., Taylor, M., Stahl, M., Malakian, K., Somers, W., Mosyak, L., Bowlby, M. R., Chanda, P., and Rhodes, K. J. (2004) *Neuron* **41,** 587–598
6. Nadal, M. S., Ozaita, A., Amarillo, Y., Vega-Saenz de Miera, E., Ma, Y., Mo, W., Goldberg, E. M., Misumi, Y., Ikehara, Y., Neubert, T. A., and Rudy, B. (2003) *Neuron* **37,** 449–461
7. Jerng, H. H., Qian, Y., and Pfaffinger, P. J. (2004) *Biophys. J.* **87,** 2380–2396
8. Serodio, P., and Rudy, B. (1998) *J. Neurophysiol.* **79,** 1081–1091
9. Dixon, J. E., Shi, W., Wang, H. S., McDonald, C., Yu, H., Wymore, R. S., Cohen, I. S., and McKinnon, D. (1996) *Circ. Res.* **79,** 659–668
10. Zhou, W., Qian, Y., Kunjilwar, K., Pfaffinger, P. J., and Choe, S. (2004) *Neuron* **41,** 573–586
11. Hasdemir, B., Fitzgerald, D. J., Prior, I. A., Tepikin, A. V., and Burgoyne, R. D. (2005) *J. Cell Biol.* **171,** 459–469
12. Jerng, H. H., Pfaffinger, P. J., and Covarrubias, M. (2004) *Mol. Cell Neurosci.* **27,** 343–369
13. Shibata, R., Misonou, H., Campomanes, C. R., Anderson, A. E., Schrader, L. A., Doliveira, L. C., Carroll, K. I., Sweatt, J. D., Rhodes, K. J., and Trimmer, J. S. (2003) *J. Biol. Chem.* **278,** 36445–36454
14. Pioletti, M., Findeisen, F., Hura, G. L., and Minor, D. L., Jr. (2006) *Nat. Struct. Mol. Biol.* **13,** 987–995
15. Wang, H., Yan, Y., Liu, Q., Huang, Y., Shen, Y., Chen, L., Chen, Y., Yang, Q., Hao, Q., Wang, K., and Chai, J. (2007) *Nat. Neurosci.* **10,** 32–39
16. Holmqvist, M. H., Cao, J., Hernandez-Pineda, R., Jacobson, M. D., Carroll, K. I., Sung, M. A., Betty, M., Ge, P., Gilbride, K. J., Brown, M. E., Jurman, M. E., Lawson, D., Silos-Santiago, I., Xie, Y., Covarrubias, M., Rhodes, K. J., Distefano, P. S., and An, W. F. (2002) *Proc. Natl. Acad. Sci. U. S. A.* **99,** 1035–1040
17. Muchmore, D. C., McIntosh, L. P., Russell, C. B., Ancerson, D. E., and Dahlquist, F. W. (1989) in *Methods in Enzymology* Vol. 177, pp. 44–73, Academic Press
18. Ou, H. D., Lai, H. C., Serber, Z., and Dotsch, V. (2001) *J. Biomol. NMR* **21,** 269–273
19. Reese, M. L., and Dötsch, V. (2003) *J. Am. Chem. Soc.* **125,** 14250–14251
20. Pervushin, K., Riek, R., Wider, G., and Wuthrich, K. (1997) *Proc. Natl. Acad. Sci. U. S. A.* **94,** 12366–12371
21. Nietlispach, D., Ito, Y., and Laue, E. D. (2002) *J. Am. Chem. Soc.* **124,** 11199–11207
22. Salzmann, M., Pervushin, K., Wider, G., Senn, H., and Wuthrich, K. (1998) *Proc. Natl. Acad. Sci. U. S. A.* **95,** 13585–13590
23. Salzmann, M., Wider, G., Pervushin, K., Senn, H., and Wuthrich, K. (1999) *J. Am. Chem. Soc.* **121,** 844–848
24. Zhu, G., Kong, X. M., and Sze, K. H. (1999) *J. Biomol. NMR* **13,** 77–81
25. Ottiger, M., Delaglio, F., and Bax, A. (1998) *J. Magn. Reson.* **131,** 373–378
26. Zweckstetter, M., and Bax, A. (2000) *J. Am. Chem. Soc.* **122,** 3791–3792
27. Losonczi, J. A., Andrec, M., Fischer, M. W., and Prestegard, J. H. (1999) *J. Magn. Reson.* **138,** 334–342
28. Schwede, T., Kopp, J., Guex, N., and Peitsch, M. C. (2003) *Nucleic Acids Res.* **31,** 3381–3385
29. Roosild, T. P., Greenwald, J., Vega, M., Castronovo, S., Riek, R., and Choe, S. (2005) *Science* **307,** 1317–1321
30. Bartels, C., Xia, T., Billeter, M., Güntert, P., and Wüthrich, K. (1995) *J. Biomol. NMR* **6,** 1–10
31. Keller, R. (2004) *The Computer Aided Resonance Assignment Tutorial*, Cantina Verlag, CH-6410 Goldau
32. Dominguez, C., Boelens, R., and Bonvin, A. M. (2003) *J. Am. Chem. Soc.* **125,** 1731–1737
33. Koradi, R., Billeter, M., and Wuthrich, K. (1996) *J. Mol. Graph.* **14,** 51–55, 29–32
34. Berkefeld, H., Sailer, C. A., Bildl, W., Rohde, V., Thumfart, J. O., Eble, S., Klugbauer, N., Reisinger, E., Bischofberger, J., Oliver, D., Knaus, H. G., Schulte, U., and Fakler, B. (2006) *Science* **314,** 615–620
35. Fakler, B., Brandle, U., Glowatzki, E., Weidemann, S., Zenner, H. P., and Ruppersberg, J. P. (1995) *Cell* **80,** 149–154
36. Osawa, M., Dace, A., Tong, K. I., Valiveti, A., Ikura, M., and Ames, J. B. (2005) *J. Biol. Chem.* **280,** 18008–18014
37. Ames, J. B., Hendricks, K. B., Strahl, T., Huttner, I. G., Hamasaki, N., and Thorner, J. (2000) *Biochemistry* **39,** 12149–12161
38. Wishart, D. S., and Sykes, B. D. (1994) *J. Biomol. NMR* **4,** 171–180
39. Prestegard, J. H., al-Hashimi, H. M., and Tolman, J. R. (2000) *Q. Rev. Biophys.* **33,** 371–424
40. Tjandra, N., Omichinski, J. G., Gronenborn, A. M., Clore, G. M., and Bax, A. (1997) *Nat. Struct. Biol.* **4,** 732–738
41. Tjandra, N., and Bax, A. (1997) *Science* **278,** 1111–1114
42. Berjanskii, M. V., and Wishart, D. S. (2005) *J. Am. Chem. Soc.* **127,** 14970–14971
43. Berjanskii, M., and Wishart, D. S. (2006) *Nat. Protoc.* **1,** 683–688
44. Baker, K. A., Hilty, C., Peti, W., Prince, A., Pfaffinger, P. J., Wider, G., Wuthrich, K., and Choe, S. (2006) *Biochemistry* **45,** 1663–1672
45. Zhou, P., Lugovskoy, A. A., and Wagner, G. (2001) *J. Biomol. NMR* **20,** 11–14
46. Morohashi, Y., Hatano, N., Ohya, S., Takikawa, R., Watabiki, T., Takasugi, N., Imaizumi, Y., Tomita, T., and Iwatsubo, T. (2002) *J. Biol. Chem.* **277,** 14965–14975
47. Beck, E. J., Bowlby, M., An, W. F., Rhodes, K. J., and Covarrubias, M. (2002) *J. Physiol.* **538,** 691–706
48. Venters, R. A., Farmer, B. T., 2nd, Fierke, C. A., and Spicer, L. D. (1996) *J. Mol. Biol.* **264,** 1101–1116
49. Gardner, K. H., Rosen, M. K., and Kay, L. E. (1997) *Biochemistry* **36,** 1389–1401